Int. J. Multiphase Flow Vol. 19, No. 2, pp. 295–307, 1993
Printed in Great Britain.

0301-9322/93 $6.00 + 0.00

AN ANNULAR FLOW MODEL FOR PREDICTING LIQUID CARRYOVER INTO AUSTENITIC SUPERHEATERS

S. A. FISHER[1] and D. L. PEARCE[2]

[1]Department of Chemical Engineering, Imperial College of Science, Technology and Medicine, London SW7 2BY, England

[2]PowerGen plc, Ratcliffe Technology Centre, Ratcliffe-on-Soar, England

(Received 15 May 1991; in revised form 29 November 1992)

Abstract—The presence of liquid water in austenitic superheaters can lead very rapidly to stress corrosion failures when the water contains salts like sodium hydroxide, commonly used to protect the ferritic evaporator sections of once-through boilers. Careful control of water chemistry and the use of a volatile alkaline water treatment can reduce the risks to a low level, but consideration must still be given to the possiblity of faults arising in operating systems where the chemical control could deteriorate for short periods. Complete protection can still be given, however, if it is possible to ensure that no wetting of the austenitic surfaces can take place. To ensure this, it is necessary to allow sufficient margins of superheat to completely evaporate any liquid water carrying over from the last stages of the evaporators. Unless great care is taken to set the smallest possible margins, however, this can prove to be very expensive in lost boiler output. This paper describes an annular flow model which represents the steam/water flows in serpentine evaporators in sufficient detail to locate the final disappearance of liquid films at the wall and the position of complete dryout. It is based on the annular flow model of Fisher & Pearce, expanded not only to include the evaporation from the liquid films and entrained droplets but also to take into account the thermal non-equilibrium caused by the presence of dry surfaces. The model gives predictions in very good agreement with localized dryout patterns observed throughout a fully pressurized steam/water serpentine evaporator.

Key Words: horizontal annular flow, evaporator, dryout, stress corrosion

1. INTRODUCTION

The presence of liquid water in austenitic superheaters can lead to very rapid stress corrosion failures when the water contains salts like sodium hydroxide, commonly used to protect the ferritic evaporator sections of boilers. For once-through boilers, the boiler water chemistry is very carefully controlled to avoid such problems, e.g. by utilizing volatile alkaline water treatment, generally based on ammonia, to ensure that the risk is low (Bignold & Penfold 1989). For an operating plant, however, consideration must still be given to the possibility of a fault causing standards to fall. The time involved need not be long for serious damage to occur. At New Huls power station in 1958, for example, failures of this kind occurred within 20 min of the superheaters becoming wetted (Baerlecken & Lorenz 1958).

Though the risks are small, extra safeguards are desirable. One such safeguard can be provided by operating the superheaters with sufficient superheat margins at the ferritic/austenitic transition joints for any liquid carrying over from the evaporators to be fully evaporated before it reaches the austenitic materials. One way of choosing such margins has been to estimate the degree of superheat needed to evaporate the largest remaining drop. This poses a number of problems, but one approach is to first assume that throughout there is thermodynamic equilibrium between the steam and water phases, to obtain the position where a thermodynamic quality of 1.0 is achieved. A very rough estimate can then be made of where in relation to this the last large drops might originate and sufficient allowance to be given to ensure that even the largest drops will evaporate before the transition joint is reached; the largest drop diameter being estimated from a turbulence model. However, in practice it is not the case that the vapour and liquid remain in thermal equilibrium, because of the presence of dry superheated surfaces which can begin to appear quite early in the evaporator stages. It also turns out not to be a simple matter to estimate the maximum size of the droplets when there are bends present. Bends can collect the largest droplets at the walls and when liquid films are thereby created more drops can be re-entrained from such films back into the vapour, with increased diameters. Simple droplet models can underestimate droplet sizes, therefore, and so provide optimistic levels of the superheat margin. High levels of superheat can

be chosen to ensure adequate safety margins, but unfortunately this can then be very costly in terms of lost boiler output.

A more accurate method is needed, therefore, than those afforded by simple droplet models. This paper describes an annular flow representation, including liquid re-distribution by the bends, which enables the final disappearance of liquid films at the wall to be determined along with a realistic location for the true position of complete dryout. By revealing the appearance and extent of any dry patches, the model can also allow for non-equilibrium superheating of the vapour phase and the consequent evaporation of droplets. This, together with the inclusion of the interchanges between the droplets and liquid films, gives a more representative calculation of the remaining quantities of liquid.

The authors also believe that because chemical attack at the wall is extremely unlikely without the presence of an actual liquid film, safe, but much less restrictive, operating conditions can be adopted—ensuring the absence of liquid films rather than the evaporation of drops. Such a criterion is simple to define and is more readily verified in practice than conditions expressed in terms of numbers and sizes of droplets. The annular flow representation, which enables such a condition to be determined, has been checked against measured results. The basic model was tested thoroughly and directly in air and water models by Fisher & Pearce (1978) and the expanded model, described below, is further checked by comparing its predictions of localized dryout patterns with those observed throughout a serpentine evaporator pressurized to 149 bar.

2. THE ANNULAR FLOW MODEL

The annular flow model of Fisher & Pearce (1978) was, in part, similar to others derived for *vertical* annular flows, with thin wavy films of liquid flowing along the walls driven by the fast flowing vapour tearing droplets from wave crests and carrying them along in the vapour core. For horizontal tubes, however, the flows are much more complicated, with rapid draining from the upper surfaces down the sides, resulting in very thin films at the top and thick films at the bottom of the tubes. There has always been much speculation on how the films at the top of the tube could be maintained. Fisher & Pearce (1978), after making comprehensive observations on horizontal annular flows, argued that no special mechanisms need be considered. It is simply that at the tube top the liquid films are so thin that there is virtually no loss of liquid from there by the entrainment of droplets into the vapour. Most of the drops in the vapour core, making up roughly 50% of the total liquid, originate from the large waves in the bottom of the tube. On the other hand, because the entrained drops are rapidly diffused across the vapour core, they are re-deposited back onto the walls over the whole circumference. The transfer of liquid from the bottom of the tube to the top arises, therefore, simply as a balance between that draining from the top surface down the walls and that returned to it as "rain" originating mainly from the waves flowing along the bottom (figure 1).

The Fisher & Pearce (1978) model represented all these processes and was thoroughly tested against measurements of film thickness and flow rate made in an air/water facility over the complete circumference of horizontal tubes of bores 12, 19, 32 and 51 mm. Very good agreement was obtained between predictions and measurements at the tube top and bottom walls. Only in the difficult regions at the sides, were there significant errors. Since then others have attempted to introduce additional flow mechanisms to improve the representation at the sides (Laurinat *et al.* 1985; Jepson 1988) but, as will be justified later, the authors do not believe that such additions are required here. It *is* necessary, however, to expand this earlier model to deal not only with the initial appearance of partial dryout (the limit of the earlier paper) but also to be able to continue modelling on into the regions where the dry surfaces become extensive and thermal non-equilibrium is significant. This is because the increased thermal resistance between dry surfaces and vapour causes the dry surfaces to superheat, which in turn causes superheating of the vapour. There will then be evaporation of the droplets into the superheated vapour. A further complication is that bends can collect droplets and so cause re-wetting of the walls. These will dry out again, probably within the next horizontal pass. This wetting and drying continues until there is too little liquid left to re-form any liquid films. Eventually, there is complete evaporation of all the remaining droplets. It has been usual in evaporator calculations, to allow the "final dryout" location (i.e. where the walls finally stay completely dry) to be located somewhere before a thermodynamic

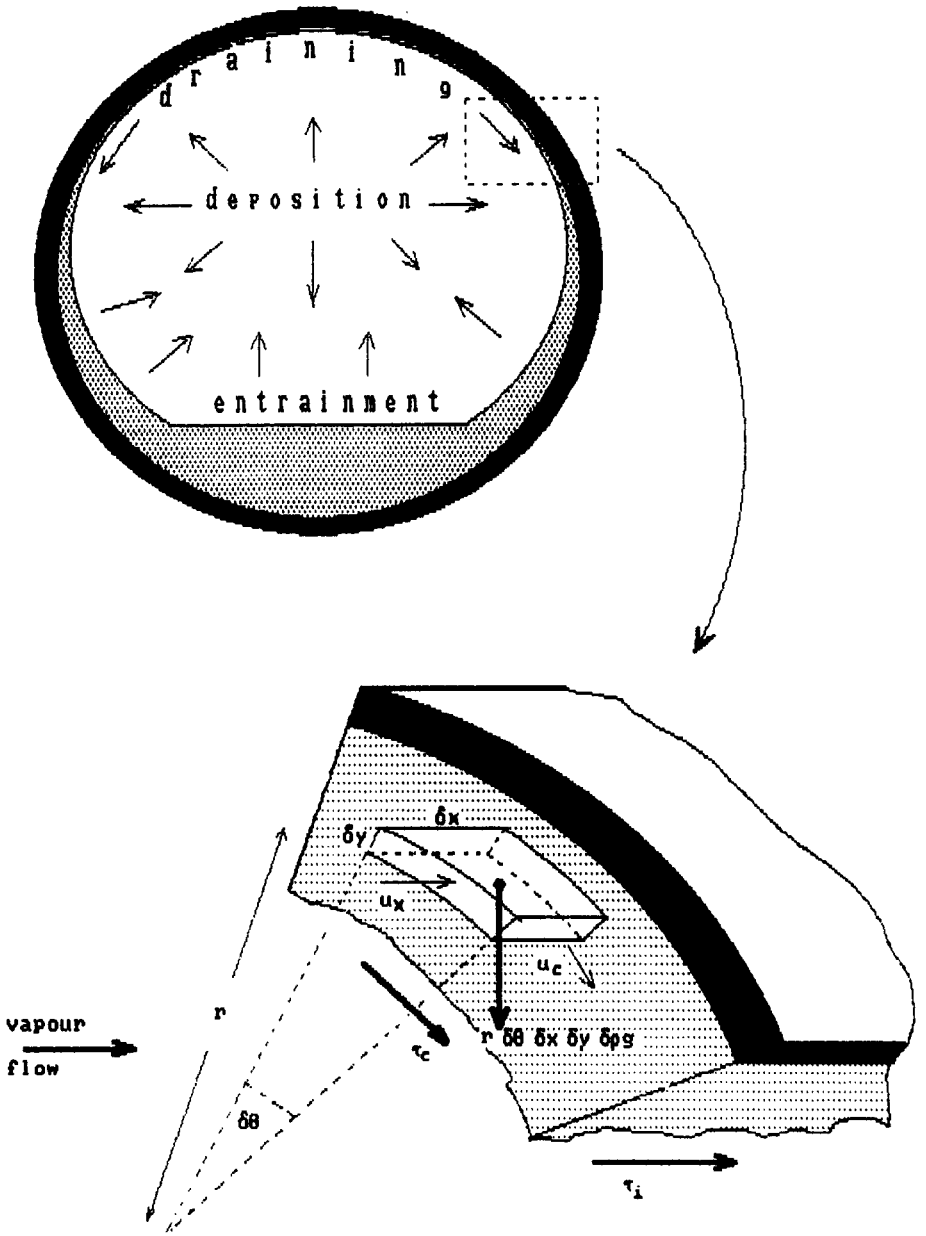

Figure 1. The annular flow model, illustrating the liquid draining and replenishment mechanisms and showing the forces and flows for a small element of the liquid film.

quality of 1.0 is reached. No theory has been offered to predict this location and, on tenuous grounds, a steam quality of 0.7 has been adopted commonly for the condition defining this point. The complete dryout of all the remaining drops, has been assumed to have taken place when a thermodynamic quality of 1.0 is reached. In practice, however, there is evidence of the existence of liquid films staining the walls of evaporators up to and beyond this. The model described here deals with these matters.

The essential flow mechanisms at work in these horizontal annular flows are summarized below, before the numerical solution procedure is outlined in section 3. To be able to deal with all the thermohydrodynamic effects the expanded model includes:

- Film drainage.
- Axial/circumferential thinning/thickening of films.
- Entrainment of droplets into the vapour core.

- Droplet deposition from the vapour core onto the film.
- Evaporation from the liquid films and droplets.
- The formation of dry surfaces and the consequent superheating of vapour from these localized dry surfaces.
- Re-wetting and re-distribution of films in bends.

The wavy nature of the films is taken into account only by implication in the use of the published correlations for the entrainment of droplets from the films (see section 2.3 below) and for the pressure drop.

The computational method centres on solving the continuity equation for mass flows in and out of the film, in a sector of angular size $\delta\theta$ and an axial length δx (figure 1). The mass flows across the film boundaries in a sector must satisfy the continuity equation

$$\frac{1}{R}\frac{\partial \Gamma_c}{\partial \theta} + \frac{\partial \Gamma_x}{\partial x} + \frac{Q}{\Delta H} - D + E = 0, \qquad [1]$$

where R is the tube radius, Γ_c is the local circumferential drainage of the film and Γ_x is the local axial flow (kg m^{-1} s^{-1}), given by

$$\Gamma_c = \rho_L \int_0^a u_c \, dy \quad \text{and} \quad \Gamma_x = \rho_L \int_0^a u_x \, dy.$$

Here a is the liquid film thickness (m), ρ_L is the liquid density (kg m^{-3}) and u_c and u_x are the circumferential and axial liquid velocities, respectively (m s^{-1}); D is the droplet deposition rate (kg m^{-2} s^{-1}), E is the entrainment rate (kg m^{-2} s^{-1}), Q is the wall heat flux (W m^{-2}) and ΔH is the "effective" latent heat, given by

$\Delta H_{LG} + \Delta H_{sup}$ if the steam is superheated or

ΔH_{LG} if there is thermal equilibrium.

Changes are assumed to take place sufficiently slowly for continuity to be satisfied throughout and so for the ith angular sector from the top of the jth axial sector along the tube

$$\frac{\Gamma_{c(i+1)} - \Gamma_{c(i)}}{R\delta\theta} + \frac{\Gamma_{x(j+1)} - \Gamma_{x(j)}}{\delta x} + \frac{Q_{ij}}{\Delta H} - D_j + E_{ij} = 0. \qquad [2]$$

The terms in the above equations are described in the next section under individual headings, before the numerical procedures are outlined in section 3.

2.1. Film drainage

The film drainage in the thin liquid film can be assumed to be a creeping flow and so for the element shown in figure 1 a force balance can be given by

$$\frac{\partial \tau}{\partial y} + \rho_L g \sin\theta - \frac{\partial p}{\partial \theta} = 0, \qquad [3]$$

where p is the pressure (Pa) and τ is the circumferential shear stress (N m^{-2}).

Others have included inertia terms and wave-spreading mechanisms (Laurinat *et al.* 1985; Jepson 1988). For simplicity these were not written in here and the justification for this will be seen later, but the model could be so enhanced if it proved to be necessary.

Substituting for the pressure gives

$$\frac{\partial \tau}{\partial y} + \Delta\rho g \sin\theta + \frac{\sigma}{R}\frac{\partial\left(\frac{1}{r}\right)}{\partial \theta} = 0, \qquad [4]$$

where σ is the surface tension (N m^{-1}) and g is the acceleration due to gravity (m s^{-2}). Integrating with respect to y

$$\tau + y\left[\Delta\rho\, g \sin\theta + \frac{\sigma}{R}\frac{\partial\left(\frac{1}{r}\right)}{\partial \theta}\right] = \text{const.} \qquad [5]$$

At the liquid film/vapour interface there will be a negligible circumferential shear stress caused by the difference in velocity between the draining liquid film and vapour but when droplets impinge there will be a net momentum loss from the film because of the need to accelerate such droplets circumferentially up to the film draining speed (Fisher & Pearce 1978). In effect this is a drag on the surface of the film and can be represented by a circumferential interfacial surface shear

$$\tau_c = Du_i, \qquad [6]$$

where D is the droplet deposition rate.

Usually, surface tension effects can be neglected and [5] can be integrated to give

$$\tau = (a - y)(\Delta\rho g \sin\theta) + \tau_c. \qquad [7]$$

The form given by Nusselt for external film steam condensation, where a is the liquid film thickness (mm).

The shear stress [7] is integrated to give the draining velocity profile (see appendix A) and, bearing in mind that

$$\tau = \mu\left(1 + \frac{\epsilon}{v}\right)\frac{\partial u}{\partial y}$$

where u is the film velocity (m s^{-1}), ϵ is the eddy diffusivity, μ is the dynamic and v the kinematic viscosity of the liquid, the film draining, Γ_c, is obtained by integrating the circumferential velocity profile across the film

$$\Gamma_c = \mu \int_0^{a^+} u^+ \, dy^+ \qquad [8]$$

and back-calculating to achieve overall continuity of flow. a^+, y^+ and u^+ are the non-dimensional forms of a, y and u, i.e. au^*/v, yu^*/v and uu^*/v, respectively, where u^* is the friction velocity.

The draining profile is subjected to an upper limit on velocity so that it cannot exceed the free-fall velocity

$$[2gr(1 - \cos\theta)]^{1/2}.$$

2.2. *Axial flows in the film*

The liquid films, though quite thin, are very turbulent because of the axial flows and so, after Butterworth (1973), it is assumed that

(a) The turbulence is homogeneous.
(b) The von Karman universal velocity profile applies in the axial direction of the film at each circumferential position.
(c) The axial shear stress is constant across the film (see Fisher & Pearce 1978).

The axial flow rate at each circumferential and axial position is obtained by integrating the universal velocity profiles across the film (see appendix A):

$$\Gamma_x = \mu \int_0^{a^+} w^+ dy^+, \qquad [9]$$

where w^+ is the non-dimensional form of the axial velocity, wv^*/v.

The solutions depend on the interfacial shear stress, which is here assumed to be constant around the circumference [following Fisher & Pearce (1978)], but variations could be allowed without difficulty.

2.3. *Droplet entrainment and deposition*

There are no widely established theoretical methods for calculating droplet entrainment or deposition rates. The approach adopted here, therefore, is to take the simplest plausible relationships and to then test their effectiveness by application of the overall model.

A number of empirical correlations have been published for entrainment, such as the rationalizations of Sugarawa (1988), but they cannot yet be recommended for pressurized steam/water

conditions. For the time being, therefore, a correlation is used based on a least-squares fit to the data of Whalley & Hewitt (1978) of the form

$$\frac{E\sigma}{\tau_i \mu} = F\left(\frac{\tau_i a}{\sigma}\right), \quad [10]$$

where τ_i is the axial interfacial shear stress (see appendix A).

For deposition, Sugarawa (1988) offered a model based on the assumption that droplet deposition was analogous to the rate of heat transfer. It seems to result in deposition rates which are unreasonably high for pressurized steam/water systems.

Whalley & Hewitt (1978) suggested a simple relationship,

$$D = kC_E, \quad [11]$$

where C_E is the droplet concentration (kg m^{-3}). The deposition coefficient, k, is given by

$$k = \frac{87\, u_h^* \mu_L}{(d\sigma\rho_L)^{1/2}} \quad [12]$$

and u_h^*, the friction velocity, is based on the homogeneous vapour core density.

Here, a more simple approach is adopted and k is obtained as an empirical correlation coefficient to the data of Whalley & Hewitt (1978). The gravitational drift is estimated to be small for the conditions of interest, and so in view of the simplicity of the model used, the deposition rate, D, is assumed to be uniform over the whole circumference.

For a homogeneous flow of vapour and entrained droplets

$$C_E = \rho_L \dot{m}_e \left(\frac{\dot{m}_e}{\rho_L} + \frac{\dot{m}_G}{\rho_G}\right)^{-1}, \quad [13]$$

where m_e is the mass flow rate of the entrained liquid and ρ_G is the vapour density.

2.4. Re-distribution of liquid by the bends

For serpentine evaporators it is necessary to include the effect of the return bends on the liquid flows, because within the bends the larger drops will be swept onto the walls and the liquid films will be re-distributed (usually the bends are not heated in power station evaporators). Here it is assumed that *all* the droplets are swept onto the walls by the bends and that the resulting liquid film is uniformly spread at the start of each horizontal pass. Neither of these two conditions will be precisely correct in practice and other liquid distributions can be applied. This model was adopted here for its simplicity and after computations had indicated that fully developed distributions of liquid would be established well before the next bend, and so it was believed the choice would not be critical.

3. NUMERICAL SOLUTION OF THE CIRCUMFERENTIAL DRAINING AND AXIAL FLOWS

The computations require unavoidably complicated numerical iterations. It would not be appropriate to attempt to describe all the details of the method used in a paper of this nature, but the essential stages are outlined. In principle it is a simple approach, solving the continuity equation for liquid mass flows into and out of the film.

Boiling can be included readily, but more than simply allowing for evaporation is needed and so, for clarity, this is left to be discussed in the next section.

Consideration of the equations for film flows and the droplet entrainment and deposition rates, given in appendix A, shows that, generally, at any axial position it is the entrainment and film thickness distributions which have to be found. When these are known at any axial location, the effect of any elemental axial change can be calculated and the entire new circumferential film distribution obtained. Starting computations immediately behind a bend at the beginning of a horizontal pass, the uniform film thickness, a, will be known and so the entrainment rate and the axial flow can be calculated. It is then a simple matter to move a small distance axially along the

tube and allow for the loss due to entrainment. At the very top of the tube there will be no draining. Moving away from the top of the tube around the circumference will require a loss from draining [8]. At each infinitesimal section (see figure 1) the inflows/outflows from the neighbouring sections, both alongside and upstream/downstream, are known and so for each a mass balance can be drawn up. For axial positions after the start of the horizontal pass there will also be a need to include a component for the deposition of droplets arising from the liquid fraction entrained in the vapour from the upstream sections. New film thicknesses, and hence entrainment rates and axial flows, can be calculated and this process is continued around the circumference until the bottom of the tube has been reached. The first attempt will not give the same overall axial flow as that determined directly from the total flow less the entrained fraction, because the changes introduced in the film thickness give rise to changes in the circumferential distribution of the axial flows. It is necessary to back-calculate, therefore, until an overall correct mass balance has been achieved. This takes only about 10 iterations and the calculation can then proceed to the next axial section where there will be a new entrained fraction. The best choice of angular and axial displacements for the calculations to proceed efficiently depends on the rate at which film thicknesses are changing, the accuracy required and the computational capability. The authors found it necessary here not only to choose the axial displacements carefully with regard to the evaporator conditions but also to have a numerical procedure where the steps changed as the calculations progressed along the tube.

The solutions for the film thickness distributions arising from the foregoing analysis sometimes show a sharp peak at the very bottom of the tube. This is a legitimate solution but one that does not seem to occur in practice, except behind large waves in very erratic flows like surging flows (Fisher *et al.* 1978). What actually happens in annular flows is that the liquid at the bottom of the tube builds up as a "flat" surface, where there is a balance between the droplets falling onto it and the liquid flowing into it (both axially and circumferentially), with that leaving by droplet entrainment and axial flow alone. This condition results in deeper bottom films at higher ambient pressures (Pearce 1982). For example, at a liquid density ratio of 4:1 in Freon-12 at 30 bar (equivalent to 178 bar in steam/water), the authors have observed flows, classically annular in character, with wall films and much droplet entrainment, but with liquid streaming along the tube bottom at times up to one-third of the tube diameter deep.

To deal with this possibility, a numerical test is incorporated at every axial station to detect "incipient peaking" and when this is indicated it is replaced by a flat surface. The depth of liquid is determined by the program itself as that required to satisfy the mass balances. This again is an iterative process carried out until the required solution is achieved.

Evaporation and the other effects of heating are considered in the next section.

4. HEATING AND NON-EQUILIBRIUM THERMODYNAMICS

The effect of heating and vaporization can be included in continuity [1] and [2] and without difficulty in the subsequent numerical analyses outlined in section 3. However, this is not sufficient in itself once dry patches begin to appear. This will be when the liquid replenishment mechanisms at any point on the inner surfaces of the tube fail to provide sufficient liquid to make up for that lost by evaporation, re-entrainment and draining at that point. Once formed, the dry surface will superheat to a level determined by the increased thermal resistance and this in turn will lead to superheating of the vapour in contact with it. Such effects are usually ignored and it is a common practice to assume thermodynamic equilibrium throughout evaporators. This requires there to be complete evaporation of all the liquid once there has been sufficient heat absorbed overall for a thermodynamic quality of 1.0 to be reached. That this is not always so is difficult to demonstrate at high steam/water pressures but liquid *has* been directly observed in experimental facilities in the form of drops at levels of thermodynamic quality >1.0 (Caplin *et al.* 1989). To deal with such effects the numerical model first detects the presence of any dry wall, by testing when the wetting mechanisms supply less liquid than is being lost, as mentioned above. It then calculates the level of superheat at the wall, the resulting superheat of the vapour and the subsequent evaporation of droplets into the superheated vapour. For an accurate account to be taken of the thermodynamic

imbalance in the latter stages of the evaporator the authors have found it necessary to include the effects of dry surfaces as soon as they appear. The annular flow model computations must be started, therefore, at least several passes before dry surfaces are indicated (an example, describing the occurrence of dry surfaces, is given in section 5).

Most of the heat falling onto or generated in a sector of tube wall with an inner dry surface passes directly into the steam, except for that lost as latent heat to evaporate droplets raining onto it at a rate insufficient to cause wetting. However, a correction *is* needed to allow for heat conducting circumferentially around the tube to any wet and, therefore, cooler surface. An exact treatment is avoided in this already complex numerical procedure and the circumferential heat flux is assumed to be given simply by the temperature difference between the wet (T_{wet}) and dry (T_{dry}) surfaces, divided by twice the wall thickness (t):

$$Q_{cond} = \lambda_{tube}\left(\frac{T_{dry} - T_{wet}}{2t}\right); \qquad [14]$$

λ_{tube} is the thermal conductivity of the tube wall ($W\,m^{-1}\,K^{-1}$).

Checks on this simple expression show it to give reasonable results and it has the necessary condition of zero wall conduction when there is no wet or dry patch. The details for determination of the heat fluxes from the wet and dry walls are given in appendix B.

The turbulent mixing in the vapour is assumed to be sufficient to ensure uniform vapour temperature at any cross section. Other relationships needed for calculating the heat and mass transfers are given in appendix B. The simplest treatments regarded as sufficient for these purposes were adopted. The drop size is averaged over the whole population and it is assumed here that all droplets are moving at three-quarters the steam speed, which is conservative for heat transfer considerations.

5. COMPARISONS OF PREDICTIONS WITH HIGH-PRESSURE STEAM/WATER DATA

There are no published reports, known to the authors, on direct measurements of liquid under superheated or near-superheated conditions in steam/water at high pressures, though as mentioned earlier, Caplin *et al.* (1989) have described seeing many water droplets in superheated steam at 160 bars at thermodynamic qualities >1.0. However, patterns of dry patches have been described in some detail in a serpentine steam/water evaporator operating at 149 bar (Crow *et al.* 1979). Such patterns are predicted by the model described here and so they provide a comprehensive test, though an indirect one, of the model proposed. Crow *et al.* (1979) made detailed measurements of wall circumferential temperatures at many stations along the straight lengths and in most of the bends. Using a rapid-response UV recorder, they took great care to measure and analyse the temperature data in ways that would indicate where dryout was to be found at the inner wall surfaces and reported detecting dry patches beginning to appear at upper surfaces well down in the evaporator. There was re-wetting in the bends to start with and the patches became larger in each pass until dryout appeared at the bottom as well as at the top and eventually the walls stayed completely dry. They could not publish all the details but they have since very kindly supplied to the authors, a complete set of results for one condition.

The serpentine had a uniform bore of 22.1 mm, a pass length of 3.17 m and the return bends were alternately 57 and 133 mm in diameter. The evaporator was heated electrically through the walls by joule heating, with a heat flux varying from 60 to 65 kW/m^2, carefully matched to a part load distribution for an operating boiler. The results for a flow of 552 $kg/m^2\,s$ and a pressure of 149 bar are shown in figure 2. A steady dry surface was first detected along the upper surface of the evaporator at a thermodynamic quality of 0.76, towards the end of pass 36. The predicted result agrees closely. Rewetting was observed after the following bend with a dry surface reappearing, again along the top, in the next pass, but starting nearer the inlet as predicted. All the bends were observed to cause rewetting up to the exit of pass 42, after which all the surfaces remained dry.

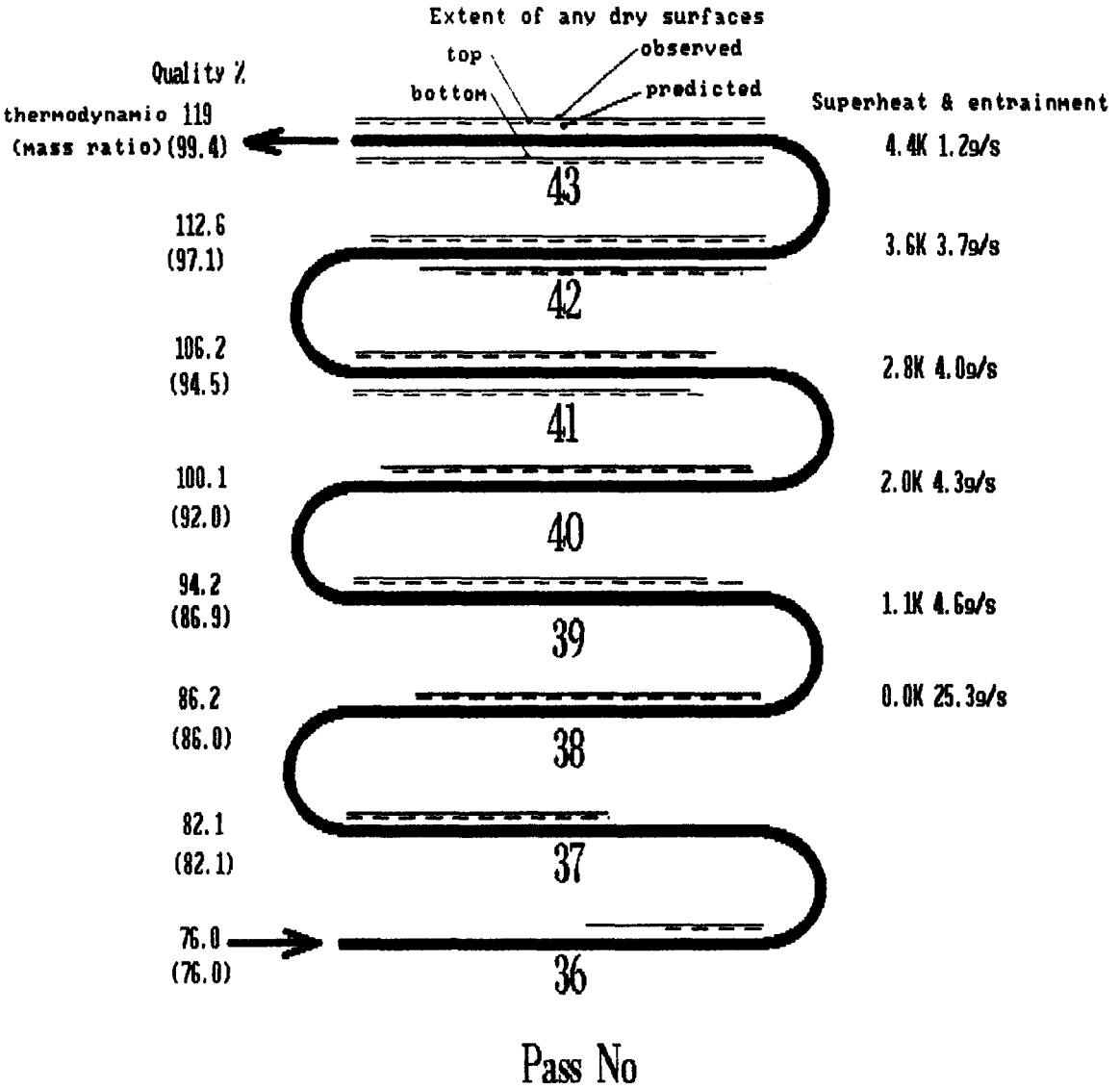

Figure 2. Comparison of the observed and predicted incidences and extent of dry surfaces, which first appear in pass 36 of a multipass steam/water serpentine evaporator.

The first occurrence of a steady dry surface along the tube bottom was observed in pass 41 and, again, this is in agreement with the prediction. Indeed, the predicted and observed patterns agree well throughout and it is particularly encouraging that these patterns match for both the bottom as well as the top surfaces.

This comprehensive confirmation of the annular flow model predictions is quite remarkable in view of the simple correlations used for entrainment and deposition, bearing in mind that no points of agreement were imposed in any way. Sensitivity calculations were carried out, therefore, changing the rates of entrainment and deposition by arbitrary factors. The effect of any significant change in these rates was to cause a lack of convergence in the numerical computations.

For further information, figure 2 also includes calculated results, for the inlet of each pass, showing how once dry surfaces start to appear the predicted vapour mass fraction begins to lag behind the thermodynamic quality calculated assuming thermodynamic equilibrium between phases. Vapour superheats are given and can be seen to be finite before a 100% thermodynamic quality is reached. Thin liquid films continue after the thermodynamic quality reaches 100% and some entrained liquid droplets are predicted to survive after the tube surfaces have beome completely dry.

6. CONCLUSIONS

1. A fluid flow model has been proposed fully describing annular flows in serpentine evaporators for conditions up to the complete evaporation of all the liquid.
2. In tests of the model, very good agreement was shown between predicted and observed dryout patterns in a high-pressure steam/water evaporator operating at 149 bar up to complete dryout.
3. The annular flow model can be used to predict superheat margins in once-through evaporators which will avoid liquid carryover into the superheater stages.
4. The model can be used to determine where liquid films will no longer be able to form at the walls and so, in conjunction with the choice of water chemistry, it will support the most economic way of setting margins to avoid the risk of corrosive attack at the inner surfaces of evaporators and superheaters.

Acknowledgements—This paper is published by kind permission of PowerGen plc and includes material researched by its forerunner, the Central Electricity Generating Board.

REFERENCES

BAERLECKEN, E. & LORENZ, K. 1958 Stress corrosion and development of the structure with the austenitic chrome–nickel steel. *Mitt. V. G. B.* **54,** 215–264.

BIGNOLD, G. J. & PENFOLD, D. 1989 Feedwater chemistry targets for ions of low volatility. CEGB Report.

BUTTERWORTH, D. 1973 An analysis of film flow for horizontal annular flow and condensation in a horizontal tube. AERE Harwell Report R7575.

CAPLIN, J. N., DENNETT, G. F. & COXON, I. J. 1989 Water droplet carryover in a serpentine steam generator tube. CEGB Report.

COLBURN, A. P. 1933 A method of correlating forced convection heat transfer data and a comparison with fluid friction. *Trans. AIChE* **29,** 174–178.

CROW, I., GREENE, J. C., TYLDESLEY, J. D. & WALKER, M. A. 1979 The behaviour of certain feedwater solutes in a high-pressure once through boiler. *Proc. Inst. Mech. Engrs* **193,** 349–354.

DAVIS, E. J. & DAVID, M. M. 1964 Two phase gas–liquid convection heat transfer. *Ind. Engng Chem. Fundam.* **3,** 111–118.

FISHER, S. A. & PEARCE, D. L. 1978 A theoretical model for describing horizontal annular flows. Paper presented at an *Int. Semin. for Momentum Heat and Mass Transfer in Two-phase Energy and Chemical Systems*, Dubrovnik.

FISHER, S. A., HARRISON, G. S. & PEARCE, D. L. 1978 Premature dryout in conventional and nuclear power station evaporators. Paper presented at the *6th Int. Conf.*, Toronto.

HEAT TRANSFER and FLUID FLOW SERVICE (HTFS) 1981 Two-phase pressure drop. Design Report 28, Harwell and NEL, East Kilbride.

JEPSON, W. P. 1988 Liquid film thickness variation in horizontal annular flow in large diameter pipes. AERE Report R12991.

LAURINAT, J. E., HANRATTY, T. J. & JEPSON, W. P. 1985 Film thickness distribution for gas–liquid annular flow, in a horizontal pipe. *PhysicoChem. Hydrodynam.* **6,** 179–195.

LIS, J. & KELLARD, P. O. 1968 A review of recent data on superheated steam. CEGB Report.

LOCKHART, R. W. & MARTINELLI, R. C. 1949 Proposed correlation of data for isothermal two-phase, two component flow in pipes. *Chem. Engng Prog.* **45,** 39–48.

MCADAMS, W. H. 1954 *Heat Transmission*, 3rd edn, pp. 129–140. McGraw-Hill, New York.

PEARCE, D. L. 1982 Two-phase flow regimes in horizontal tubes: an experimental investigation of flow regimes in Refrigerant-12, HTFS Research Symposium Paper HTFS RS429, AERE Harwell.

SUGARAWA, S. 1988 Droplet deposition and entrainment modelling based on the three fluid model. Paper presented at the *3rd Int. Top. Mtg on Nuclear Power Plant Thermal Hydraulics and Operations*, Seoul.

WHALLEY, P. B. & HEWITT, G. F. 1978 The correlation of liquid entrainment fraction and entrainment rate in annular two-phase flow. Reports AERE R9187 and HTFS RS237.

WOODFORD, D. J. 1989 Droplet carryover in serpentine evaporators. CEGB Report.

APPENDIX A

Axial and Drainage Flows

Axial flows

The universal velocity profile is:

$$\text{for } y^+ \leqslant 5, \qquad w^+ = y^+; \tag{A1a}$$

$$\text{for } 5 < y^+ \leqslant 30, \qquad w^+ = 5 \ln y^+ - 3.05; \tag{A1b}$$

and

$$\text{for } y^+ > 30, \qquad w^+ = 2.5 \ln y^+ + 5.5. \tag{A1c}$$

The friction velocity, $u^* = (\tau_i/\rho_L)^{1/2}$, is based on the vapour/liquid film interfacial axial shear stress, τ_i. This can be calculated, using either the Lockhart & Martinelli (1949) or HTFS (1981) correlations, or measured values can be used, for example, to allow for any circumferential variation of axial shear stress (see Fisher & Pearce 1978).

The eddy diffusivity profile becomes:

$$\text{for } y^+ \leqslant 5, \qquad \frac{\epsilon}{\nu} = 0; \tag{A2a}$$

$$\text{for } 5 < y^+ \leqslant 30, \qquad \frac{\epsilon}{\nu} = \frac{y^+}{5} - 1; \tag{A2b}$$

and

$$\text{for } y^+ > 30, \qquad \frac{\epsilon}{\nu} = \frac{y^+}{2.5} - 1. \tag{A2c}$$

The axial flow is obtained by integrating the axial velocity profile [A1] across the film:

$$\text{for } y^+ \leqslant 5, \qquad \Gamma_x = \frac{\mu a^{+2}}{2}; \tag{A3a}$$

$$\text{for } 5 < y^+ \leqslant 30, \qquad \Gamma_x = \mu a^+(5 \ln a^+ - 8.05) + 12.5; \tag{A3b}$$

and

$$\text{for } y^+ > 30, \qquad \Gamma_x = \mu a^+(2.5 \ln a^+ - 3) - 64. \tag{A3c}$$

Draining flows

The shear stress [7] can be integrated to give the draining velocity profile:

$$\text{for } y^+ \leqslant 5, \qquad u^+ = y^+\left[\left(Ba^+ - \frac{\tau_c}{\tau_i}\right) - By^+\right]; \tag{A4a}$$

$$\text{for } 5 < y^+ \leqslant 30, \qquad u^+ = 5\left[\left(Ba^+ - \frac{\tau_c}{\tau_i}\right)(\ln y^+ - 0.61) - B(y^+ - 2.5)\right]; \tag{A4b}$$

and

$$\text{for } y^+ > 30, \qquad u^+ = 2.5\left[\left(Ba^+ - \frac{\tau_c}{\tau_i}\right)(\ln y^+ + 2.18) - B(y^+ - 25\right]; \tag{A4c}$$

where

$$B = \frac{\nu g\, \Delta\rho \sin\theta}{(\rho_L u^{*3})},$$

as used by Butterworth (1973), and bearing in mind that

$$\tau = \mu\left(1 + \frac{\epsilon}{\nu}\right)\frac{\partial u}{\partial y},$$

the film draining, Γ_c, is obtained by integrating the circumferential velocity profile across the film:

for $y^+ \leqslant 5$,

$$\Gamma_c = \mu a^{+2}\left(\frac{Ba^+}{3} - \frac{\tau_c}{\tau_i}\right); \quad \text{[A5a]}$$

for $5 < y^+ \leqslant 30$,

$$\Gamma_c = 5\mu\left\{B[a^{+2}(\ln a^+ - 2.11) + 5a^+ - 4.167] - \frac{\tau_c}{\tau_i}[a^+(\ln a^+ - 1.61) + 2.5]\right\}; \quad \text{[A5b]}$$

and

for $y^+ > 30$,

$$\Gamma_c = 5\mu\left\{B[a^{+2}(\tfrac{1}{2}\ln a^+ + 0.341) - 25a^+ + 220.8] + \frac{\tau_c}{\tau_i}[\tfrac{1}{2}a^+(\ln a^+ - 0.591) + 12.5]\right\}. \quad \text{[A5c]}$$

APPENDIX B

Evaporation and Non-equilibrium Thermodynamics

The drop size is averaged over the whole population and is given by the Weber number:

$$\mathrm{We} = \frac{\rho_G \Delta V^2 d_{drop}}{\sigma} = 20, \quad \text{[B1]}$$

where ΔV is the velocity difference between the steam and droplets. It is assumed here, conservatively, that all the droplets are moving at three-quarters of the steam speed.

The number of drops in a slice of vapour core of length δx is

$$\delta n = \tfrac{3}{2}\left(\frac{d_{tube}^2}{d_{drop}^2}\right)\frac{\delta x}{\left(1 + \dfrac{\dot{m}_G \rho_L \beta}{\dot{m}_e \rho_G}\right)} \quad \text{[B2]}$$

where, β, the droplet/vapour velocity ratio is 0.75 (Woodford 1989). The surface area of all the drops in the slice is $\delta A = \pi d_{drop}^2 \delta n$. The heat transfer to the droplets is given by a Nusselt number relationship:

$$\mathrm{Nu} = 2 + 0.196\left(\frac{d_{tube}}{d_{drop}}\right)\mathrm{Re}^{0.602}, \quad \text{[B3]}$$

where Re, the Reynolds number, is the vapour core value (Woodford 1989).

The sensible heat transfer between the liquid film and the superheated vapour is given by the Dittus–Boelter correlation (e.g. McAdams 1954):

$$\mathrm{Nu} = 0.023\ \mathrm{Re}^{0.8}\mathrm{Pr}^{0.4}, \quad \text{[B4]}$$

where the Reynolds number, Re, and Prandtl number, Pr, are taken for the dry superheated steam conditions.

The heat balance for the superheated flow becomes

$$Q = \dot{m}_G \frac{\partial H_{sup}}{\partial x} + \Delta T\left(h_{drop}\frac{\partial A_{drop}}{\partial x} + \pi d_{tube} h_{film} F_{wet}\right), \quad \text{[B5]}$$

where $\Delta T = T_{sup} - T_{sat}$, $Q = Q_{dry}\pi d_{tube}(1 - F_{wet})$ and F_{wet} is the fraction of the tube surface wetted.

To make the computations as simple as possible the steam enthalpy is linearized:

$$H_{sup} = H_{sat} + c_H \Delta T, \quad \text{[B6]}$$

where c_H is the rate of change of superheated enthalpy (J kg^{-1} K^{-1}). The steam temperature rise, δT, in an axial distance δx is

$$\delta T = \frac{\delta x}{\dot{m}_G c_H}\left\{Q - \pi d_{tube}\,\Delta T\left[\frac{3}{2}\frac{d_{tube}}{d_{drop}}\frac{h_{drop}}{\left(1+\frac{\dot{m}_G \rho_l \beta}{\dot{m}_e \rho_G}\right)} + h_{film} F_{wet}\right]\right\}, \quad [B7]$$

where h_{drop} and h_{film} are the heat transfer coefficients at the drop and film surfaces, respectively (W m^{-2} K^{-1}), and β is the phase velocity ratio.

The change in superheat is computed using this equation across every axial section following every dry patch, even if the wall subsequently re-wets, provided the vapour remains superheated. A back-calculation based on the temperature change then gives the steam enthalpy and ultimately the thermodynamic quality.

The heat transfer coefficients for the wet and dry surfaces are determined from standard correlations.

For the wet wall (Davis & David 1964):

$$h_{wet} = 0.060\frac{\lambda_{film}}{d}\,Re_{DD}^{0.87}\,Pr_{film}^{0.4}\left(\frac{\rho_{film}}{\rho_{sup}}\right)^{0.28}, \quad [B8]$$

where ρ_{sup} is the vapour density,

$$Re_{DD} = \frac{(dG_{tot}X_{flow})}{\mu_L},$$

d is the tube diameter (m) and λ_{film} is the thermal conductivity of the liquid film, G_{tot} is the total mass flux and X_{flow} is the quality of the flowing steam/water mixture.

For the dry wall (Lis & Kellard 1968):

$$h_{dry} = 0.00925\frac{\lambda_{Tdry}}{d}\,Re_{Tdry}^{0.871}\,Pr_{Tdry}\left[\frac{\rho_{sup}}{\rho_{Tdry}}\right]^{0.139}, \quad [B9]$$

where Re_{Tdry} is based on the superficial velocity of the vapour and the subscript Tdry refers to the superheated dry vapour conditions. For a dry wall, a heat balance can be written in terms of the Nusselt numbers, Nu, leading to:

$$T_{dry} - T_{wet} = \frac{Nu_{dry}}{Nu_{dry}+1}\left(\frac{Q}{h_{dry}} + T_{sup} - T_{wet}\right), \quad [B10]$$

where

$$Nu_{dry} = \frac{h_{dry}s_{dry}}{\lambda_{tube}}$$

and s_{dry} is the dry perimeter (m).

For a wet wall, there is a similar heat balance, which gives:

$$T_{wet} = \frac{Nu_{dry}T_{sup}\left[1+\frac{Q}{h_{dry}T_{sup}}\right] + Nu_{wet}T_{sat}\left[1+\frac{Q}{h_{wet}T_{sat}}\right](1+Nu_{dry})}{Nu_{dry} + Nu_{dry}Nu_{wet} + Nu_{wet}}, \quad [B11]$$

where

$$Nu_{wet} = \frac{h_{wet}s_{wet}}{\lambda_{tube}}$$

and s_{wet} is the wet perimeter.

T_{wet} and T_{dry} can be determined thus for each axial station and the effective heat fluxes from the wet and dry surfaces found.